Prediction of Drug Distribution in Subcutaneous Xenografts of Human Tumor Cell Lines and Healthy Tissues in Mouse: Application of the Tissue Composition-Based Model to Antineoplastic Drugs

PATRICK POULIN,[1] YUNG-HSIANG CHEN,[2] XIAO DING,[2] STEPHEN E. GOULD,[3] CORNELIS ECA HOP,[2] KIRSTEN MESSICK,[4] JASON OEH,[3] BIANCA M. LIEDERER[2]

[1]Consultant, Québec City, Québec, Canada
[2]Drug Metabolism and Pharmacokinetics, Genentech Inc., South San Francisco, California 94080
[3]Translational Oncology, Genentech Inc., South San Francisco, California 94080
[4]In Vivo Study Group, Genentech Inc., South San Francisco, California 94080

Received 19 November 2014; revised 5 December 2014; accepted 12 December 2014

Published online 14 January 2015 in Wiley Online Library (wileyonlinelibrary.com). DOI 10.1002/jps.24336

ABSTRACT: Advanced tissue composition-based models can predict the tissue–plasma partition coefficient (K_p) values of drugs under *in vivo* conditions on the basis of *in vitro* and physiological input data. These models, however, focus on healthy tissues and do not incorporate data from tumors. The objective of this study was to apply a tissue composition-based model to six marketed antineoplastic drugs (docetaxel, DOC; doxorubicin, DOX; gemcitabine, GEM; methotrexate, MTX; topotecan, TOP; and fluorouracil, 5-FU) to predict their K_p values in three human tumor xenografts (HCT-116, H2122, and PC3) as well as in healthy tissues (brain, muscle, lung, and liver) under steady-state *in vivo* conditions in female NCR nude mice. The mechanisms considered in the tissue/tumor composition-based model are the binding to lipids and to plasma proteins, but the transporter effect was also investigated. The method consisted of analyzing tissue composition, performing the pharmacokinetics studies in mice, and calculating the corresponding *in vivo* K_p values. Analyses of tumor composition indicated that the tumor xenografts contained no or low amounts of common transporters by contrast to lipids. The predicted K_p values were within twofold and threefold of the measured values in 77% and 93% of cases, respectively. However, predictions for brain for each drug, for liver for MTX, and for each tumor xenograft for GEM were disparate from the observed values, and, therefore, not well served by the model. Overall, this study is the first step toward the mechanism-based prediction of K_p values of small molecules in healthy and tumor tissues in mouse when no transporter and permeation limitation effect is evident. This approach will be useful in selecting compounds based on their abilities to penetrate human cancer xenografts with a physiologically based pharmacokinetic (PBPK) model, thereby increasing therapeutic index for chemotherapy in oncology study. © 2015 Wiley Periodicals, Inc. and the American Pharmacists Association J Pharm Sci 104:1508–1521, 2015

Keywords: ADME; chemotherapy; oncology; disposition; distribution; partition coefficients; pharmacokinetics; PBPK modeling; tumor; xenograft

INTRODUCTION

The efficacy and toxicity of antineoplastic drugs in the treatment of tumors is highly dependent on the ability of the drugs to distribute into tumor tissue at the optimal therapeutic dose. Guidance provided by the regulatory agencies recommends safe starting doses in humans[1]; however, the lack of certain preclinical data, particularly dose/concentration response curve predictions in both plasma and tumors, limits the strength of such guidance. In other words, guidance in chemotherapeutic pharmacokinetics (PK) would significantly improve if predictions of drug dosimetry in neoplastic tissues could be made. This information would undoubtedly improve dosing regimens and create

Abbreviations used ADME, absorption distribution, metabolism, and elimination; BCRP, breast cancer resistance protein; hBCRP-MDCKII, MDCKII-cells that overexpress human wild-type BCRP; mBcrp1-MDCKII, MDCKII-cells that overexpress mouse wild-type BCRP1; CA, cardiolipin; CE, cholesterylester, Cer, ceramides; Cerebr, cerebrosides; Chol, cholesterol; CCC, concordance correlation coefficient; DCM, dichloromethane; DG, diacylglycerol; DOC, docetaxel; DOX, doxorubicin; ELSD, evaporative light scattering detector; ESI, electrospray ionization; FAME, fatty acid methyl ester; FFA, free fatty acid; F_{cells}, fractional content of cells in tissues; F_{inters}, fractional content of interstitial space in tissues; F_{nl}, fractional content of neutral lipids equivalent; F_{apl}, fractional content of acidic phospholipids equivalent; F_{pr}, fractional content of binding proteins; F_w, fraction of water equivalent; fu_p, unbound fraction in plasma; 5-FU, fluorouracil, GC–MS, gas chromatography–mass spectrometry; GEM, gemcitabine; hENT1, human nucleoside transporters; HCT-116, human colon adenocarcinoma cell line; H2122, human non-small cell lung adenocarcinoma; *I*, ionization term; Inters, interstitial; K_p, tissue–plasma partition coefficient; K_{pu}, tissue–plasma water partition coefficient for the unbound drug; log *P*, log *n*-octanol–water partition coefficient; LPC, lysophosphatidylcholine; LPE, lysophosphatidylethanolamine; MDCKI parental, Madin-Darby canine kidney strain I parental cells; MDCKII parental, Madin-Darby canine kidney strain II parental cells; MeOH, methanol; MG, monoacylglycerol; MRP2, multidrug resistance-associated protein 2; MRP2-MDCKII, MDCKII-cells overexpressing wild-type MRP2; MS, mass spectrometry; MSTFA, N-methyl-N-(trimethylsilyl)trifluoroacetamide); MTBE, methyl tert-butyl ether; m/z, mass-to-charge ratio; MTX, methotrexate; NaCl, sodium chloride; NaOMe, sodium methoxide; OATP, organic anion-transporting polypeptide of the member family 1B1, 1B3 or 2B1; *P*, partition coefficient; PBPK, physiologically based pharmacokinetics; PK, pharmacokinetics; PK/PD, pharmacokinetic–pharmacodynamic; PC3, human prostate cancer cell line; PC, phosphatidylcholine; PE, phosphatidylethanolamine; PI, phosphatidylinositol; PS, phosphatidylserine; Pgp, p-glycoprotein; p*K*a, ionization constant; P_{nl}, neutral lipid–aqueous phase partition coefficient; P_{apl}, acidic phospholipid–aqueous phase partition coefficient; P_{pr}, protein–aqueous phase partition coefficient; TG, triacylglycerol; Tof, time of flight; TOP, topotecan; UPLC, ultra-performance liquid chromatography; V_{ss}, volume of distribution at steady state.

Correspondence to: Dr. Patrick Poulin (Telephone: +418-802-3985; E-mail: patrick-poulin@videotron.ca)

Journal of Pharmaceutical Sciences, Vol. 104, 1508–1521 (2015)

more efficacious chemotherapy. The basic assumption in *in vivo* pharmacokinetic–pharmacodynamic (PK/PD) chemotherapeutic research relies on the assumption that the unbound drug levels at the site of action are the relevant measure of drug effect. Accordingly, toxicities and efficacies seem to be driven by drug tissue concentrations rather than by free drug plasma concentrations.[2] Therefore, the importance of tumor tissue partitioning on drug PK properties can be recognized. In this case, it becomes imperative to develop a prediction model to select compounds based on their abilities to penetrate tumors, thereby increasing the therapeutic index. Furthermore, the prediction model would benefit if the prediction of total and free drug concentration into tissues/tumors can be made separately whether the later matrices of drug concentration are related to toxicity or efficacy. At the present time in drug discovery, however, the estimation of drug penetration in tumors is mostly performed under resource intensive *in vivo* conditions in human cancer xenografts models.

Alternatively, physiologically based pharmacokinetic (PBPK) models are well suited for the simulation of concentrations within individual tissues. Up to now, however, approaches for predicting the essential tissue–plasma partitioning data for input into the models has focused mostly on healthy (normal) tissues.[3–15] An extension of the recently developed prediction approaches from healthy tissues to tumors becomes the necessary next step in circumventing the time-consuming process of growing tumors in nude mice. Poulin et al.[3] recently examined tissue–plasma partitioning relationships using healthy tissues and human tumor xenograft models in mouse, resulting in correlation formulas for predicting tumor tissue–plasma partition coefficient (K_p) values for various compound ionization classes on the basis of only healthy tissue K_p values determined *in vivo*. The principle of correlation analysis has been successfully validated in veterinary, toxicology, and PK studies for steady-state and non-steady-state conditions and for various routes of administration [intravenous (i.v.), oral, and/or intraperitoneal].[4–12] In general, the linearity of correlations may indicate similar distribution mechanisms in both healthy and tumor tissues, which can help in the development of a more mechanistic approach for predicting K_p values.

In this context, advanced tissue composition-based models, which utilize a combination of human *in vitro* measurements, physicochemical data, and physiological data to predict tissue distribution have been developed, negating the need for animal *in vivo* data.[15,16] The tissue composition-based model is described in a way that it can be used to predict tumor tissue partitioning at both the total and free drug level (i.e., partitioning into the aqueous, lipid and protein compartments can be estimated separately), and, hence, could be related to toxicity and efficacy end points. These tissue composition-based models, which were first developed for healthy tissues, can be applied to tumor tissues as the corresponding tumor composition data become available. The distribution mechanisms currently considered in these models are the binding to lipids and to plasma proteins in each tissue compartment. The next logical step is, therefore, to determine whether these mechanisms could also be of importance in the prediction of drug penetration, particularly into human tumor xenografts in female NCR nude mice. Furthermore, the effect of transporters and their contribution to drug resistance should be investigated because transporters can be expressed in tumor cells.[17–19] Several authors have investigated the contribution of transporters versus binding to lipids and proteins to the overall distribution of a drug, but these studies have principally involved healthy tissues.[3,6,13–15]

The objective of this study was to apply the mechanistic tissue composition-based model to three human tumor xenografts (HCT-116, H2122, and PC3) to predict K_p values determined under steady state, *in vivo* conditions in female NCR nude mice for six marketed antineoplastic drugs: docetaxel (DOC), doxorubicin (DOX), gemcitabine (GEM), methotrexate (MTX), topotecan (TOP), and fluorouracil (5-FU). K_p predictions for healthy tissues (brain, muscle, lung, and liver) were determined in parallel. In effect, this was a first attempt to develop a tissue composition-based model for diverse human tumor xenografts in mouse by comparing the model's predictive performance to K_p values determined under *in vivo* conditions.

METHOD

The composition of healthy tissues and tumors was analyzed, *in vivo* tissue distribution studies in mouse were performed, and observed K_p values were predicted. In addition, tissue composition analyses established the abundance of lipids and common transporter families in the human tumor xenografts in order to determine whether the transporter effect or binding to lipids is the predominant distribution mechanism. Finally, *in vitro* transport studies were performed to further analyze the predictions.

Test Compounds

A total of six marketed antineoplastic drugs were considered in this study (DOC, DOX, GEM, MTX, TOP, and 5-FU). The chemical structures of these compounds are diverse, and the group includes charged bases and acids as well as uncharged (neutral) molecules at physiological pH as characterized by the ionization constant (p*K*a). For these drugs, the observed unbound fraction in plasma (fu_p) ranged from 0.012 to 0.99, the lipophilicity (log *n*-octanol–water partition coefficient; log *P*) ranged from −0.89 to 4.26, and the volume of distribution at steady state in mouse ranged from 0.25 to more than 50 L/kg; therefore, the current dataset covers a large range of physicochemical and tissue distribution properties[20–26] (Table 1).

Experimental Studies

A description of each experimental method is detailed in the Appendix as supplementary information; however, a brief description of each experiment is presented below.

Tissue Lipid Composition Data

The composition of lipids in the studied healthy tissues and human tumor xenografts was experimentally determined in female NCR nude mice by lipodomic analyses.[27] These experiments were performed in collaboration with the VTT Technical Research Centre of Finland as described in the Appendix. For the purpose of this study, diverse types of lipids were analyzed, namely, neutral lipids [ceramides, cerebrosides (Cerebr), cholesterol (Chol), cholestheryl esters, fatty acids, and tryglycerides], neutral phospholipids (phosphatidylcholine, lysophosphatidylcholine, phosphatidylethanolamine, lysophosphatidylethanolamine, sphingomyeline, and plasmalogens), and ionized lipids [phosphatidylserine (PS) and phosphatidylinositol (PI)]. The data are reported in mg lipids/g wet

Table 1. Test Set of Compounds

Drugs	Class	p*K*a	Log *P*	fu_p[a]	RBP[b]	V_{ss} (L/kg)[c]	Blood CL (mL/min kg)[c]	Eh[d]	P_{app} Ratio (B–A/A–B[e] MDR1-MDCKI	P_{app} Ratio (B–A/A–B[e] MDCKII-mBcrp
DOC	Neutral	–	4.26	0.012	1.16	9	23	0.19	142	9
DOX	Base	8.3	1.27	0.235	4.70	>50	11	0.09	26	33
GEM	Base	3.6	−1.4	0.99	1.49	2.14	27	0.23	0.7	8
MTX	Acid	4.7	−1.08	0.796	2.71	0.63	15	0.12	1	8
TOP	Zwitterion	6.99_{acid} 10.5_{base}	−0.30	0.65	1.02[b]	3.99	83.3	0.69	41	72
5-FU	Acid	8.1	−0.89	0.88	1	0.25	54.3	0.45	2.1	3.3

CL, clearance; DOC, docetaxel; DOX, doxorubicin; Eh, hepatic extraction ratio; 5-FU, fluorouracil; fu_p, unbound fraction in plasma; GEM, gemcitabine; log *P*, log *n*-octanol–water partition coefficient; MTX, methotrexate; p*K*a, ionization constant; RBP, blood–plasma ratio; TOP, topotecan; V_{ss}, volume of distribution at steady state.

[a] Determined in this study by using the dialysis technique. Preclinical studies confirm that plasma protein binding of TOP is low (35%).[21]

[b] Determined in this study at the end of the infusion studies. A value of unity was assumed for 5-FU.

[c] Volume of distribution at steady-state and hepatic blood CL estimated in this study.

[d] Calculated as the ratio between hepatic blood CL and the liver blood flow rate assumed in a standard mouse (120 mL/min kg).[22–26]

[e] *In vitro* transport studies as described in the method.

tissue weight and by fractional content of wet tissue weight (Table 2). All classes of lipids were considered to estimate the lipid binding effect in the tissue composition-based model.

Transporter Abundance

The abundance of common transporter families in each human tumor xenografts in female NCR nude mice was experimentally determined by membrane protein extraction and total protein quantification as reported in the literature.[28] These experiments were performed in collaboration with the Department of Pharmaceutics at the University of Washington. The abundance of the following transporters was measured: p-glycoprotein (Pgp), breast cancer resistance protein (BCRP), multidrug resistance-associated protein 2 (MRP2), and organic anion-transporting polypeptide of the 1B1 (OATP1B1), 1B3 (OATP1B3), and 2B1 (OATP2B1) families. The data are reported in fmol/μg of membrane protein (Table 3). Even though these transporters cover a broad range of membrane-localized transporters, other families of transporters are known to govern drug penetration in healthy and tumor tissues in female NCR nude mice (e.g., the human nucleoside transporters (hENT1) for GEM).[29] Because of the limited capacity, the effect of these additional transporters was assumed to be negligent.

In vitro Transport Studies

The six drugs were tested for efflux in Madin-Darby canine kidney (MDCK) cells that overexpress the above transporter families in order to determine whether these drugs undergo transport. The method is detailed in the Appendix.

In Vivo Tissue Distribution Studies

The drug concentration in healthy tissues, tumor xenografts, and plasma was experimentally determined under steady-state *in vivo* conditions after continuous i.v. administration of each drug in female NCR nude mice (a 7 h infusion with MTX at 0.3731 mg/h and GEM at 1.3889 mg/h, an 8 h infusion with DOC at 7.0 mg/h, a 17 h infusion with TOP at 0.10 mg/h, and a 72 h infusion with DOX at 0.0125 mg/h). The tissues were collected for bioanalytical analyses at the end of each infusion. These experimental studies were performed at Genentech as described in the Appendix, with the exception of the K_p value *in vivo* of 5-FU in the HCT-116 xenograft, which was obtained from the literature.[30] Adipose tissue was not investigated in this study because the estimation of K_p values in this tissue requires an extended infusion to reach steady-state conditions.

Development of the Tissue/Tumor Composition-Based Model

The only changes made to the previously published tissue composition-based model[15] consist of adjusting the lipid composition data for healthy and tumor tissues in female NCR nude mice. The model equations (Table 4) used for predicting K_p values of the human tumor cells lines used in this study are, therefore, the same as those previously published for healthy tissues.[15] Likewise, the assumptions used in each model are the same: (1) solubilization in the aqueous phase as well as lipid and protein binding effects are predominant compared with the transporter effect in healthy tissues and tumors, especially when the transporters are absent, saturated and/or not upregulated after treatment, and (2) passive diffusion governs drug penetration into tissues and tumor xenografts in the absence of a permeation limitation effect. The first assumption was deemed valid by the minimal amount of transporters identified in the tumor xenografts and by published results that demonstrate a minimal transporter effect for similar xenografts.[3,13] In the absence of transporter effects, the free drug in plasma and tumor are in equilibrium and differ by the pH gradient, whereas the bound drug refers to the binding to lipids and plasma proteins, and, hence, the prediction of drug penetration into tumors should be facilitated in this context, and inversely. The second assumption is based on the lack of a barrier to accumulation in healthy tissues and tumor xenografts located in the subcutaneous fat pad in mouse, resulting in unhindered permeation into tissues, with the probable exception of the brain. Accordingly, it is also assumed that the drug permeability across the tumor xenografts should be uniform; however, a permeation limitation effect is less of concern under the current steady-state conditions.

Briefly, the tissue composition-based model takes into account the partitioning of a drug into diverse fractions of the cells and interstitial space in tissues.[15] The following four distinct processes were considered for predicting K_p values under *in vivo* conditions: (1) non-specific binding to neutral lipids equivalent, (2) ionic binding to acidic phospholipids, (3) binding to common plasma proteins such as albumin and/or lipoproteins,

Table 2. Lipid Composition of Healthy Tissues and Human Tumor Xenografts in Female NCR Nude Mice[a]

	Healthy Tissues (mg Lipids/g Wet Tissue Weight)				Tumor Xenografts (mg Lipids/g Wet Tissue Weight)			
	Liver	Brain	Lungs	Muscle	PC3	HCT-116	H-2122	Red blood cells
Lipids								
Cholesteryl esters (CE)	5.12 ± 1.49	9.38 ± 0.51	4.30 ± 2.06	5.28 ± 5.46	4.21 ± 1.95	1.88 ± 0.37	2.04 ± 1.55	–
Triacylglycerols (TG)	5.85 ± 1.52	13.12 ± 0.46	4.96 ± 3.61	7.10 ± 6.42	5.57 ± 2.13	2.06 ± 0.54	1.99 ± 0.84	–
Cholesterol (Chol)	2.19 ± 0.44	13.88 ± 3.22	5.28 ± 1.41	0.90 ± 0.67	2.82 ± 1.0	2.19 ± 0.27	3.35 ± 0.28	–
Ceramides (Cer)	0.18 ± 0.04	0.34 ± 0.04	0.16 ± 0.01	0.15 ± 0.01	0.19 ± 0.04	0.15 ± 0.01	0.16 ± 0.01	–
Cerebrosides (Cerebr)	blq	6.44 ± 2.16	blq	blq	blq	blq	blq	–
Total neutral lipids	13.34	43.16	14.70	13.42	12.79	6.28	7.53	–
Phosphatidylethanolamine (PE)	7.28 ± 1.42	49.46 ± 7.43	2.72 ± 0.66	1.82 ± 0.21	3.43 ± 0.29	1.85 ± 0.49	4.16 ± 0.92	–
Phosphatidylcholine (PC)	18.29 ± 2.28	39.67 ± 4.01	9.62 ± 1.61	6.79 ± 1.16	7.67 ± 0.61	2.84 ± 0.73	6.22 ± 0.10	–
Sphingomyeline (SM)	1.19 ± 0.41	2.65 ± 0.41	2.15 ± 0.34	blq	1.16 ± 0.10	0.63 ± 0.12	0.98 ± 0.11	–
Total neutral phospholipids	26.76	91.79	14.79	8.61	12.26	5.32	11.36	–
Phosphatidylinositol (PI)	2.45 ± 0.12	1.74 ± 0.13	0.45 ± 0.10	0.46 ± 0.07	0.49 ± 0.08	0.77 ± 0.21	0.95 ± 0.07	–
Phosphatidylserine (PS)	0.76 ± 0.09	2.39 ± 0.22	1.77 ± 0.20	0.76 ± 0.13	1.25 ± 0.15	1.86 ± 0.34	1.72 ± 0.32	–
Total acidic phospholipids	3.21	4.13	2.21	1.21	1.75	2.63	2.68	–
Total lipids	43.31	139.1	31.40	23.24	26.80	14.22	21.57	–
Data reported as fractional content of wet tissue weight for the tissue composition-based model								
Fractional content of neutral lipids equivalent (F_{nl})	0.0214	0.0707	0.0191	0.0160	0.0165	0.0079	0.0110	0.00257
Fractional content of acidic phospholipids equivalent (F_{apl})	0.00321	0.00413	0.00221	0.00121	0.00175	0.00263	0.00268	0.00046
Fractional content of water equivalent (F_w)	0.8034	0.927	0.893	0.854	0.89	0.844	0.853	0.662

blq, below the limit of quantitation.
[a]As detailed in the *Method* section and Appendix. Values refer to the mean ± SD ($n = 5$) or the mean only.

Table 3. Abundance of Transporter Content in the Human Tumor Xenografts in Female NCR Nude Mice*

	Transporter abundance (fmol/μg membrane)					
Tissues	Pgp	BCRP	MRP2	OATP1B1	OATP1B3	OATP2B1
Tumor xenografts						
HCT-116	blq	blq	blq	blq	blq	blq
H-2122	blq	3.4 ± 0.1	1.5 ± 0.1	blq	blq	blq
PC3	blq	blq	blq	blq	blq	blq
Test sets						
hBCRP-MDCKII	0.5 ± 0.1	10.7 ± 0.1	0.8 ± 0.1	blq	blq	blq
mBcrp1-MDCKII	0.2 ± 0.1	131.1 ± 0.6	blq	blq	blq	blq
MRP2-MDCKII	0.4 ± 0.1	blq	3.9 ± 0.4	blq	blq	blq
MDCKII parental	0.4 ± 0.1	blq	0.4 ± 0.1	nd	nd	nd
MDCKI parental	0.4 ± 0.2	blq	blq	nd	nd	nd

blq, below the limit of quantitation; nd, not determined.
*As detailed in the *Method* section and Appendix. Values refer to the mean ± SD ($n = 5$).

and (4) drug ionization in the aqueous phase equivalent. Overall, the tissue–aqueous phase partition coefficient (K_{pu}) refers to the ratio between the drug concentration in a tissue (i.e., the drug bound to tissue components and unbound in the aqueous phase) and the drug unbound concentration in the aqueous phase of the plasma at equilibrium. The K_p of each healthy tissue or tumor was calculated by the product of K_{pu} and fu_p for each drug.[15] Please refer to the original source for more details on the model equations and assumptions.[15]

Finally, the elimination of drugs can be a confounding factor in the prediction of K_p values for liver. The effect of drug elimination can lead to a lower than expected experimentally

Table 4. Equations and Input Parameters Used in the Unified Tissue Composition-Based Model[15]

Tissue Composition-Based Model	
Main equations	
$K_{pu_{tissue}} = F_{cells}K_{pu_{cells}} + F_{Inters}K_{pu_{Inters}}$	
$K_{pu_{cells}} = \frac{(1+I_{cells})F_{w,cells}+P_{nl,cells}F_{nl,cells}+I_{cells}P_{apl,cells}F_{apl,cells}+(1+I_{cells})P_{pr,cells}F_{pr,cells}}{(1+I_{cells})}$	
$K_{pu_{Inters}} = \frac{(1+I_{Inters})F_{w,Inters}+P_{nl,Inters}F_{nl,Inters}+I_{Inters}P_{apl,Inters}F_{apl,Inters}+(1+I_{Inters})P_{pr,Inters}F_{pr,Inters}}{(1+I_{Inters})}$	
$K_{ptissue} = K_{pu_{tissue}}fu_p$	
Input parameters	All drugs
	$I = 0_{neutrals}; I = 10^{pH-pKa}_{acids}; I = 10^{pKa-pH}_{bases}; I = 10^{pKa-pH} + 10^{pH-pKa}_{zwitterions}$
	$pH_{cell-tissues}7; pH_{cells-tumors}7.2; pH_{Inters-tissues}7.4; pH_{Inters-tumor}7.0$
	$P_{nl} = P_{ow}$
	Neutrals, acids, and weak bases
	$P_{pr,Inters} = \left[\frac{1}{fu_p} - 1 - \frac{P_{nl,plasma}F_{nl,plasma}}{1+I_{plasma}}\right]\frac{1}{F_{pr,plasma}}$
	$P_{pr,cells} = 0$
	$P_{apl,cells} = 0$
	$P_{apl,Inters} = 0$
	Predominantly ionized bases (at least one p$Ka \geq 7.0$):
	$P_{apl,cells} = \left[P_{erythrocytes:buffer} - \frac{(1+I_{erythrocytes})F_{w,erythrocytes}+P_{nl,erytrocytes}F_{nl,erythrocytes}}{1+I_{plasma}}\right]\frac{1+I_{p,plasma}}{I_{eryrhrocytes}F_{apl,erytrocytes}}$
	$P_{erythrocytes:buffer} = \left[(RBP - (1 - 0.45)\right]/0.45)/fu_p$
	$P_{apl,Inters} = 0$
	$P_{pr,Inters} = 0$
	$P_{pr,cells} = 0$
	$pH_{erythrocytes}7.2$

F_{apl}, fractional content of acidic phospholipids equivalent; F_{cells}, fractional content of cells in tissues; F_{Inters}, fractional content of interstitial space in tissues; F_{nl}, fractional content of neutral lipids equivalent; F_{pr}, fractional content of binding proteins (albumin for acids and weak bases and lipoproteins for neutrals); fu_p, unbound fraction in plasma; F_w, fractional content of water equivalent; I, ionization term; Inters, interstitial space; K_p, tissue–plasma partition coefficient; K_{pu}, tissue–aqueous phase partition coefficient; P_{apl}, acidic phospholipids–aqueous phase partition coefficient; pKa, ionization constant; P_{ow}, n-octanol–buffer partition coefficient; P_{nl}, neutral lipids–aqueous phase partition coefficient; P_{pr}, proteins–aqueous phase partition coefficient; RBP, blood–plasma ratio *in vitro*.

determined steady-state K_p value (i.e., K_p *in vivo* < K_p predicted). Consequently, in this study, the K_p values calculated for liver were adjusted for drugs for which the liver was assumed to be the main organ for elimination (DOC, DOX, and GEM).[20] A standard equation was used to adjust the calculated value with the tissue composition-based model [K_p predicted = K_p calculated * (1 − Eh)], where Eh is the hepatic extraction ratio (the ratio between the hepatic blood clearance (CL) determined *in vivo* and the blood flow rate to liver assumed in a standard mouse; 120 mL/min kg)[22–26] (Table 1). For drugs for which hepatic elimination is less significant, no adjustment was made (TOP and MTX).[20,21] Adjustment for hepatic elimination was not made for 5-FU as no prediction was made for this drug in the liver.

Estimation of the Drug-Specific Input Parameters

The drug-specific input parameters for the tissue composition-based model equations (Table 4) are related to lipophilicity (log P), ionization (pKa), and plasma protein binding (fu_p). The values of these parameters are summarized in Table 1.

Estimation of the Species-Specific Input Parameters

Lipid Composition. Since neutral phospholipids were assumed to behave as a mixture of 30% lipids and 70% water,[14] the fractional content of neutral lipids equivalent (F_{nl}) corresponds to the sum of all neutral lipids in addition to 30% of the content of all neutral phospholipids. Likewise, the fractional content of water equivalent (F_w) corresponds to the water content in tissue or tumor in addition to 70% of the content of all neutral phospholipids. The total water content assumed to be in a human tumor xenograft (80%) and healthy tissues (liver, 71%; muscle, 75%; brain and lung, 79%) in mouse was obtained from the literature.[15,31] Finally, the fractional content of acidic phospholipids equivalent (i.e., ionized lipids) (F_{apl}) includes PS and PI. The lipid composition data were expressed in fractional content of wet tissue weight as required for the tissue composition-based model[15] (Table 2).

Cellular Fraction, Interstitial Space, and pH. As the tissue composition-based model separately calculates the drug distribution in the cellular and interstitial fractions of a tissue, the required additional input parameters include the cellular fraction, the volume of interstitial fluid, and the associated pH for healthy tissues and human tumor xenografts in mouse. The resulting K_p value is calculated by the sum of these two compartments, as demonstrated in Table 4. For subcutaneous human tumor xenografts, the interstitial fluid volume is assumed to be equal to 20% of the total tumor volume (and hence the cell volume is about 80%),[32] whereas the corresponding volume for healthy tissues in mouse varies depending on the tissue (fraction of cells in liver, muscle, brain, and lungs are 86%, 89.7%, 83.8%, and 68.8%, respectively).[33] The pH of a cell and the interstitial fluid compartments in healthy tissues was set to 7.0 and 7.4, respectively.[15] For standard human tumor xenografts in mouse, the pH value of cells is reported to be about 7.2, but the pH of the interstitial space is more acidic at about 7.0. The tumor pH was estimated in accordance to the tumor volume observed in this study.[34–36] The pH of plasma and red blood cells was set to 7.4 and 7.2, respectively.[15]

Protein Binding Related Parameters. Plasma and interstitial fluid contain binding macromolecules that provide high-affinity

binding sites for drugs.[15,16] The $P_{pr,Inters}$ value for interstitial fluid refers to either the albumin–water partition coefficient for acidic compounds (acids and acidic zwitterions) and weak bases or the lipoprotein–water partition coefficient for neutral drugs. This parameter was obtained from information on the unbound fraction measured *in vitro* in plasma (fu_p) (Table 4). Information on the fractional content of albumin (0.0277) and lipoprotein (0.0083) in plasma in mouse was obtained from the literature.[15] For the interstitial space of healthy tissues and tumor xenografts, these parameters were estimated on the basis of the tissue–plasma albumin and tissue–lipoprotein ratios, respectively, also obtained from the literature.[16] For the healthy tissues, these ratios are equal to approximately 0.10. A similar value was used for each tumor xenograft in the absence of experimental values (note that these parameters are not sensitive as altering the value of these ratios within the range of 0.1–0.5 changed the predicted K_p values by less than 5% for the current drugs). Also note that the distribution of small molecules is typically driven by non-specific binding in tissues; however, pharmacological target binding is generally of minor relevance in terms of contribution to the volume of distribution. Binding to intracellular proteins has, therefore, not been routinely characterized in K_p prediction studies. For the strongly basic drugs in this study (one basic p*K*a $\geq$ 7), ionic binding to acidic phospholipids was assumed to be the predominant process,[15,16] and, hence, binding to plasma proteins was neglected.

Evaluation of the Predictive Performance. The prediction accuracy was assessed by comparing predicted versus mean observed K_p values. First, plots of predicted versus observed K_p values were drawn. Second, the concordance correlation coefficient (CCC) was calculated; the CCC evaluates the global degree to which pairs of predicted and observed data fall on the line of unity passing through the origin.[8] Finally, specific fold-errors of deviation between the predicted and observed K_p values (fold-error $\leq$2, $\leq$3, and $\leq$5) are presented here.

RESULTS

A total of six drugs were evaluated in the present study for the prediction of K_p value in several healthy tissues and tumor xenografts in female NCR nude mice. Data on tissue composition are presented in Tables 2 and 3, and the comparative assessments between the predicted and observed K_p values are presented in Figures 1–4.

Tissue Composition Measurement

The tumor xenografts collected from female NCR nude mice contained no or low amounts of common transporters compared with the positive control cell lines (i.e., Pgp, BCRP, MDCK, MRP2, and OATP) on a quantitative basis (Tables 2 and 3). An exception is H2122, which showed a level of BCRP and MRP2 transporters up to 50% of the level measured in the positive controls. No measurements were made to verify whether the transporter levels were upregulated after infusion under *in vivo* conditions. By contrast, analyses of tissue lipid composition showed the presence of lipids in both the tumor xenografts and healthy tissues. Therefore, this analysis indicated that levels of total lipids in healthy tissues and tumor xenografts can be ranked in the following order: brain > liver > lung > muscle, PC3 and H-2122 > HCT-116. The same pattern was observed for the content of neutral lipids and neutral phospholipids. The levels of ionized lipids in healthy tissues and tumor xenografts can be ranked in the following order: brain > liver > H-2122 > HCT-116 > lung > PC3 > muscle.

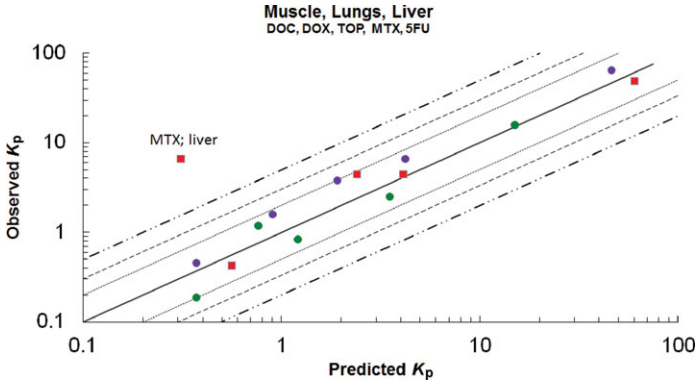

Figure 1. Predicted and observed mean K_p values for healthy tissues in mouse (muscle, lungs, and liver) for DOC, DOX, MTX, and TOP. The concordance correlation coefficient (CCC) is 0.85. The solid line indicates the best fit (unity). Dashed lines on either side of unity represent twofold, threefold, and fivefold error, respectively. The observed values refer to the mean value of 5–11 measurements (i.e., n ranges from 5 to 11) as detailed in the *Method* section and Appendix. Green; muscle, purple; lungs, red: liver.

In Vitro Transport Studies

The efflux potential of the six drugs was determined in MDR1-MDCKI and MDCKII-mBcrp cells *in vitro*. Results indicated that DOC, DOX, and TOP showed higher efflux ratios than did GEM, MTX, or 5-FU (Table 1).

In Vivo Tissue Distribution and Prediction of K_p Values

In general, the degree of drug penetration into tumor xenografts closely follows patterns in tissue composition because, in all, 93% and 77% of the predicted K_p values for healthy and tumor tissues, respectively, are within twofold error of the

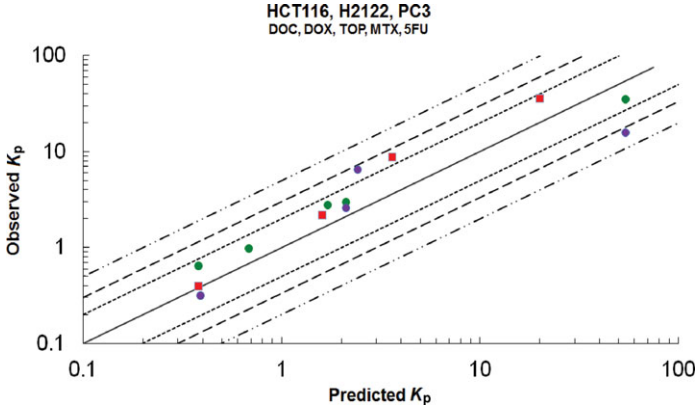

Figure 2. Predicted and observed mean K_p values for human tumor xenografts in mouse (HCT116, H2122, and PC3) for DOC, DOX, MTX, TOP, and 5-FU. The concordance correlation coefficient (CCC) is 0.93. The solid line indicates the best fit (unity). Dashed lines on either side of unity represent twofold, threefold, and fivefold error, respectively. The observed values refer to the mean value of 5–11 measurements (i.e., n ranges from 5 to 11) as detailed in the *Method* section and Appendix. Green, HCT116; purple, H2122; red, PC3.

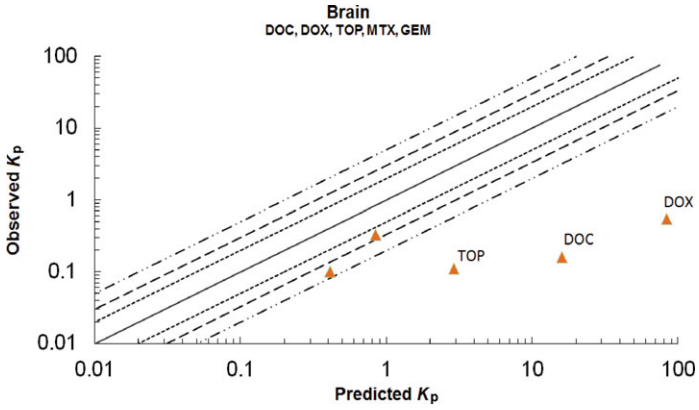

Figure 3. Predicted and observed mean K_p values for healthy tissues and human tumor xenografts in mouse for GEM. The concordance correlation coefficient (CCC) is <0.1. The solid line indicates the best fit (unity). Dashed lines on either side of unity represent twofold, threefold, and fivefold error, respectively. The observed values refer to the mean value of 5–11 measurements (i.e., *n* ranges from 5 to 11) as detailed in the *Method* section and Appendix. Yellow triangles, brain.

observed values in mouse. These numbers increase to more than 93% when considering threefold error (Figs. 1 and 2 for DOC, DOX, TOP, MTX, and 5-FU). The global coefficient of correlation is close to unity (CCC values range from 0.85 to 0.93). Accordingly, the results suggest that the tissue composition-based model developed in this study is able to provide rough estimates of drug partitioning in human tumor xenografts and healthy tissues for the current drugs. However, some discrepancies between the predicted and measured K_p values are observed. For example, no relevant penetration of GEM is observed into any tumor xenograft, in contrast to the penetration of GEM into healthy tissues. Consequently, a systematic overprediction of the *in vivo* K_p value of each tumor xenograft is reported for this drug (Fig. 3). Similarly, no relevant tissue accumulation in healthy brain tissue is observed for any drug. Again, this leads to a systematic overprediction of *in vivo* K_p values for brain (Fig. 4). Finally, the *in vivo* K_p value of liver for MTX is severely underestimated (0.35 predicted vs. 6.70 observed) (Fig. 1).

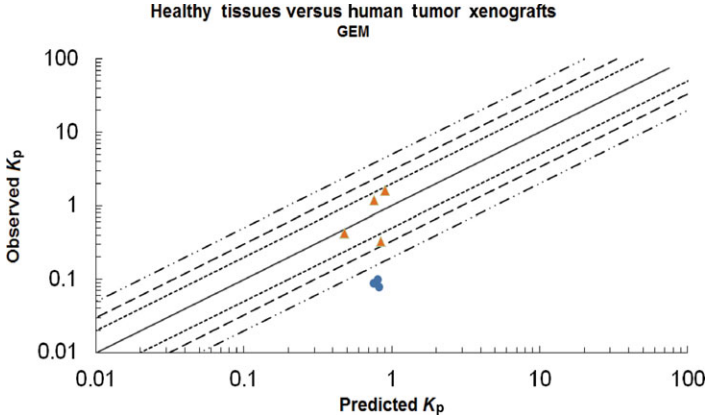

Figure 4. Predicted and observed mean K_p values for brain in mouse for DOC, DOX, MTX, TOP, and GEM. The concordance correlation coefficient (CCC) is 0.20. The solid line indicates the best fit (unity). Dashed lines on either side of unity represent twofold, threefold, and fivefold error, respectively. The observed values refer to the mean value of 5–11 measurements (i.e., *n* ranges from 5 to 11) as detailed in the *Method* section and Appendix. Yellow triangles, healthy tissues; blue circles, human tumor xenografts.

DISCUSSION

The distribution of a drug into tumors, that is, tumor accumulation, is a recognized factor in the determination of drug toxicity and efficacy[2,4]; thus, K_p values are essential parameters in preclinical and clinical oncology studies. There is a growing understanding of the physiological and biochemical factors that affect drug disposition in tissues. As such, we developed a tissue composition-based model for evaluation of tissue drug distribution under steady-state conditions by combining lipid composition data with estimates of K_p values for common human tumor xenografts in female NCR nude mice. This study was a first attempt to evaluate the tissue composition-based model for healthy tissues by comparing its predictive performance to the same model adapted for tumor xenografts. The results demonstrate that prediction of drug distribution into tumor xenografts is feasible by using six antineoplastic drugs as a proof of concept, which is in line with previous validation exercises of the tissue composition-based model,[7,15,16] and, hence, a next step would be to test this model with more antineoplastic drugs and tumor xenografts. Use of this prediction model eliminates the need to measure actual drug levels in tumors. The current approach would, therefore, speed up the selection of drug candidates by use of readily available physicochemical and *in vitro* (or *in silico*) data as input to determine whether a drug is distributed into a tumor xenograft in mouse. This is an improvement over previous prediction models that require *in vivo* experiments.[3–15] The current computational approach can be leveraged to optimize the PK drivers of tissue distribution to increase drug tumor levels and improve efficacy margins for small molecules. In addition, individual tissue-plasma K_p values can contribute to defining the overall distribution kinetics of a drug when integrated within a PBPK model, and, hence, influence the simulated curves for plasma and tumor concentrations. Tsukamoto et al.[37] successfully simulated the PK of 5-FU in a human cancer xenograft model in mouse by using a PBPK model, but the input K_p value of the tumor was experimentally determined. The ability to predict K_p values for tumors would, therefore, facilitate the development of PBPK models in oncology studies. In addition, we measured the abundance of lipids and common transporter families in the human tumor xenografts, providing comprehensive information of tumor composition. The experimental data on tissue composition support the hypothesis that lipid binding is the predominant factor governing drug distribution in the current sample of healthy and tumor tissues under steady-state *in vivo* conditions, which is the same conclusion made in prior works.[3,15] Overall, the current tissue/tumor composition-based model demonstrates the potential of predicting drug partitioning into healthy tissues and human tumor xenografts in female NCR nude mice when the predominant distribution mechanisms are the binding to lipids and binding to plasma proteins.

In this context, the results of this study indicate that the distribution of a variety of drugs in different healthy tissues and tumor xenografts under steady-state *in vivo* conditions is generally a result of non-specific binding to lipids and binding to common plasma proteins as described by the model equations

(Table 4). The findings to support the predominant impact of lipid and protein binding in drug penetration into tumor xenografts are supported by previous observations published in the literature.[3,6,13,14] Firstly, Yoshida et al.[13] and Yata et al.[14] showed high affinity for the acidic phospholipids present in both the healthy lung and lung tumor xenografts in mouse for two basic antineoplastic drugs. Interorgan variation in the content of acidic phospholipids explained the differences in K_p values across tumors and healthy tissue. Secondly, in several cases, linear regressions have been observed between healthy tissue and tumor K_p data determined under *in vivo* conditions in mouse; some authors have suggested that the magnitude of the slopes of the regression analyses approximately reflect the differences in lipid and/or protein content between the various tissues and tumors.[3,6] Tissue composition may, thus, be considered a relevant determinant of drug distribution in both healthy tissues and human tumor xenografts in mouse for the current drugs.

In general, reasonable, rough K_p predictions were obtained using the composition-based model when lipid composition was the main driver of drug tissue distribution; however, some predictions in this study showed greater than fivefold error (i.e., tumor K_p for GEM, brain K_p for each drug, and liver K_p for MTX) (Figs. 3 and 4), demonstrating the additional uncertainties that stem from the complexities of specific tissues and tumor xenografts. Several mechanisms can influence the penetration of a drug into a tissue and tumor xenograft (e.g., the transporter effect, blood flow architecture, permeation limitation, pH versus hypoxia, the elimination effect, the number of compartments) either under steady-state or non-steady-state conditions.[18,38] In the current study, the influences of altered delivery through changes in blood flow architecture and permeation limitation effect (e.g., in tumors) can probably be neglected because the current K_p values were collected at steady-state conditions. Nevertheless, a pH effect is already considered in the present calculation approach. On the other hand, no consideration of further mechanisms related to transporter and/or permeation limitation effects was made with the tissue composition-based model tested in this study, which might explain why this model provides inaccurate predictions in some cases. However, under the current steady-state conditions, the omission of a transporter effect is probably one of the most plausible explanation for the innacutate predictions compared to a permeation limitation effect.

The low abundance of common transporter families (Pgp, BCRP, MRP2, and OATP) was unanticipated in the current tumor xenografts (Table 3). This observation may explain why we were able to accurately predict the tumor K_p values in most cases by using the tissue composition-based model regardless of whether the current drugs showed affinity for these transporters[39] (Table 1). However, upregulation of transporters after multiple dosing might be observed *in vivo* (e.g., after a long infusion) and this will be examined in future studies; MRP2 expression was recently shown to increase following chemotherapy.[40] No measurements were made in this study to verify whether transporter levels were upregulated after a long infusion under *in vivo* conditions. Nevertheless, such a phenomenon is unlikely in tumor xenografts that contain no trace of transporters, which is the case for all the current xenografts, except H2122. However, BCRP and MRP2 are expressed in H2122 and could have been upregulated to some extent after long infusions in mice. Accordingly, the efflux of DOX and TOP in MDCKII-mBcrp cells (Table 1) may explain why there *in vivo* K_p values in H2122, particularly for DOX, is about twofold to threefold lower than the predicted value (16 vs. 54 in Fig. 2). Nevertheless, the good correlation between predicted and observed K_p values for most compounds (except GEM) suggests that transporters do not play a major role in this study for the tumor xenografts. It cannot be excluded that transporters are involved, but are saturated. Saturation of transporters is possible, particularly when a tumor xenograft contains a low level of transporters, which is the current situation. Essentially, as infusion proceeds, drug levels build-up in tumor xenografts and begin to progressively inhibit efflux, resulting in greater cellular sequestration over time (i.e., similar to when no transporter effect is present). For example, the literature indicates that long i.v. infusions can saturate the Pgp effect,[41] offering an additional explanation for the consistency between the predicted and observed K_p values in the tumor xenografts even if no trace of Pgp was found.

In contrast, Kalvass et al.[42] showed that saturation of Pgp in brain is unlikely as brain is assumed to highly express these transporters. Accordingly, the potential saturation effect of Pgp and/or BCRP was not observed for brain for the current drugs, and, hence, the results show that the observed brain K_p values are significantly lower than the predicted values, meaning that drug penetration in brain was unexpectedly low under *in vivo* conditions for each drug (Fig. 4). Low brain K_p values under *in vivo* conditions are in accordance with the efflux ratio measured *in vitro* in MDR1-MDCKI cells in this study, which are greater than unity for most drugs (Table 1). Accordingly, the overprediction of brain K_p values was most significant for DOC, DOX, and TOP, which showed the greatest efflux ratios. We did not estimate the abundance of the transporter families in the healthy tissues used in this study, but, according to the literature, several efflux transporters can be highly expressed in healthy brain, liver, and lung, and to a lower extent in muscle, in nude mice.[18,19,43–45] Consequently, because the brain contains a large amount of Pgp and BCRP and the current drugs are Pgp and/or BCRP substrates (Table 1),[46–50] the results indicate that an efflux effect may explain the low brain penetration observed *in vivo* for each drug. This is somewhat surprising because brain tissue is the richest in terms of lipid content, and, hence, the K_p values determined *in vivo* were expected to be much greater, but it seems that the efflux transporter effect was predominant compared to the binding to lipids. Another potential explanation for the low brain penetration is the permeation limitation effect governed by the blood–brain barrier. In this context, a previous study on lapatinib distribution demonstrated a much lower drug distribution in a metastasis located in the brain than in the same metastasis located in a peripheral organ.[51] These observations may provide insight into the function of the barrier systems in limiting drug penetration into central nervous system metastases. Lv et al.[52] demonstrated the value of an integrated PK-driven approach to identify potentially efficacious/toxic agents for brain tumor chemotherapy in rodents by the combined use of *in silico*, *in vitro* cytotoxicity, and *in vitro* absorption distribution, metabolism, and elimination profiling studies, representing a complementary approach to the tissue composition-based model for the estimation of drug penetration in brain and tumors localized in this organ. The influence of the blood–brain barrier and efflux transporter effects needs to be further investigated and taken into account in future adaptions of the tissue composition-based model.

Gemcitabine displayed a lower degree of penetration into tumor xenografts compared with healthy tissues. In other words, the observed K_p values for GEM were significantly lower than the predicted values for the tumors. On the other hand, the observed and predicted values for GEM in the healthy tissues were similar (Fig. 3). This deviation can probably be explained by transporter and/or permeation limitation effects into each tumor xenograft. As GEM is very hydrophilic ($\log P = -1.4$), the penetration of this drug into the HCT-116 xenograft is principally governed by human nucleoside transporters (hENT1).[29,39] The study results indicate that these transporters might not be expressed in the current tumor xenografts as these tumors are resistant to GEM, resulting in observed tumor K_p values that are much lower than expected under *in vivo* conditions. Accordingly, some tumor xenografts had a low number of hENT1 transporters on the cell surface (e.g., pancreatic BX-PC3),[53] and a decreased hENT1 expression in tumor tissue compared with normal tissues has been observed in humans.[54] In addition, hypoxia is commonly found in tumors as a result of the large distances that separate some neoplastic cells from the microvasculature. The high hydrophilicity of GEM may have limited its diffusion into the lipid-based membrane of the tumor xenografts in comparison with the more lipophilic drugs,[55,56] resulting in much lower K_p values than expected under *in vivo* conditions. This behavior may in part explain why GEM shows only limited efficacy in the treatment of these cancers.[29,57] Furthermore, the *in vivo* K_p value of liver for MTX is severely underestimated (0.35 predicted vs. 6.70 observed) probably because of uptake by specific hepatic transporters (e.g., folate transporters).[39,45,58]

Noteworthy challenges exist in studying drug penetration into tissue, in part due to considerable transporter effects as discussed above. In contrast, PC3 and HCT166 xenografts do not significantly express transporters[44] (Table 3), and the predicted K_p values of each drug in these tumors deviated by less than twofold error compared with the observed values. Further observations showed interanimal variability among mice xenografts in their ability to accumulate a drug, leading to variations in the current observed K_p values. For example, we observed significant variability among measured K_p values in lungs (500%) for DOC across the mice dataset (not shown), which may have affected the comparison with predicted values; lung K_p was reasonably predicted in some animals but was significantly underpredicted in others. In this case, a transporter effect (e.g., Pgp) might also be responsible for interanimal variability in the lung K_p values for DOC, as the drug penetration into lungs for DOC is governed by the Pgp transporter[18] and this drug showed high efflux ratios in MDR1-MDCKI cells in this study (Table 1). However, the nude mice used in this study should be almost genetically invariant. We also observed relative variability in tissue lipid composition in mice (Table 2), which may also be a source of interanimal variability. Variability in tissue lipid composition, however, cannot explain the variability in K_p values observed for lungs for DOC. Furthermore, the first pass effect in lung during a long i.v. infusion may cause unanticipated inflammation and drug accumulation to affect tissue distribution. As an example, a few mice in this study showed liquid accumulation, particularly in the lungs. In addition, majority of the predictions for K_p in healthy and tumor tissues were slightly underpredicted (less than observed K_p) (but they are still in good agreement with the observed values), as shown in Figures 1 and 2. A rationale for this might be that the lipid composition in different tissues and tumor xenografts was quantified in mice without drug treatment, whereas long-term i.v. infusion may potentially led to increase the amount of phospholipids but particularly into lungs for the most lipophilic strong basic drugs.[59,60] In the literature, the *in vivo* K_p values in rodents increased less than 1.5-fold with the duration of treatment for two lipophilic strong basic drugs (i.e., the K_p ratios began to rise only after 3 days of treatment).[60] In this present study, the infusion treatment was performed under a shorter period of time and lower doses were used, and, hence, a lower effect on K_p values is expected. Accordingly, in our current dataset, only DOX is relatively lipophilic and basic, whereas TOP is basic but much more hydrophilic (Table 1). Therefore, only these two drugs may potentially have induced phospholipidosis after chronic treatments in nude mice. Nevertheless, we have performed a sensitive analysis. The analysis indicates that increasing the amount of phosphoplipids by twofold in tissues and tumor xenografts increased the calculated K_p values up to twofold for DOX and TOP. The slightly higher K_p values obtained by increasing the amount of phospholipids in the tissue composition-based model are relatively in better agreement with the observed values particularly for lungs. Overall, this effect is in accordance with the literature[60] and would not affect the main conclusion of this study considering the potentially low impact for few drugs; however, a thorough assessment of the impact for the changed lipid composition on the K_p prediction might also be required. This is a next logical step; however, this is beyond the scope of the present study.

Finally, the ability to anticipate drug behavior in tumors in humans on the basis of preclinical data is a crucial expectation in oncology studies; for example, an existing preclinical model of efficacy for xenograft mice[61] would gain from the prediction of tumor K_p values. Accordingly, the tissue composition-based model is described in a way that it can be used to predict tumor tissue partitioning at both the total and free drug level (i.e., partitioning into the aqueous, lipid and protein compartments can be estimated separately) (Table 4), and, hence, could be related to toxicity and efficacy end points. Researchers have already successfully explored the interspecies differences in K_p values for healthy tissues, upholding the notion that the scaling of K_p values across species on the basis of differences in tissue composition and plasma protein binding (and the elimination effect in the case of liver) is accurate and scientifically justifiable.[4,62] For rough estimates in humans, the tissue composition of tumors can be assumed to be relatively conserved across species, and, therefore, predictions of tumor K_p in any species under steady-state *in vivo* conditions can be made by using the tissue composition-based model. The only factor that needs to be adjusted is the unbound fraction in plasma for each respective species, and this is a readily available parameter. In addition, interspecies differences in the transporter effect need to be considered when it becomes the predominant process compared with binding to lipids. Plus, as previously stated, blood flow architecture and permeation limitation would have to be considered for each species, particularly under non-steady-state conditions.[37,38]

CONCLUSIONS

Overall, the results of this study provide relevant explanations for drug penetration in healthy tissues (muscle, lung, liver, and brain) and human tumor xenografts (HCT-116, H2122, and PC3) in female NCR nude mice for six small molecules under

in vivo steady-state conditions. The tumor xenografts collected from female NCR nude mice contained no or low amounts of common transporters compared with the positive control cell lines. An exception is H2122, which showed a level of BCRP and MRP2 transporters up to 50% of the level measured in the positive controls. Therefore, drug partitioning into most of the tumors was predominantly governed by lipid and protein binding effects in addition to drug solubilization in the aqueous phase rather than the transporter effect. In other words, we have obtained reasonable predictions except when transporters and/or permeation limitation are involved (brain K_p for each drug, tumor K_p for GEM, liver K_p for MTX, lung K_p for DOC). On the other hand, an efflux Pgp transporter effect (or a permeation limitation effect) seemed to be predominant in brain tissue as none of the drugs penetrated this organ, even though the brain is rich in lipids. Thus, in the absence of transporters, the free drug in plasma and tissue are in equilibrium and differ by the pH gradient, whereas the bound drug refers to the binding to lipids and proteins, which are considered by the model. Accordingly, binding to lipids and plasma proteins as well as drug solubilization in the aqueous phase were investigated first based on the low amount of transporters found in the studied tumor xenografts. Therefore, the next logical step will be to adapt the current tissue/tumor composition-based model to incorporate also the transporter effect when this becomes the predominant mechanism. Importantly, a mechanistic tissue/tumor composition-based model was developed in this study, and the model was, in most cases, able to provide rough estimates of drug partitioning into healthy tissues and human tumor xenografts localized in the subcutaneous fat pad in nude mice. This model can predict K_p values of small molecules in healthy and tumor tissues in mouse when no transporter and permeation limitation effect is evident, which should be useful in selecting compounds based on their abilities to penetrate tissue, thereby increasing the therapeutic index for chemotherapy. This study is a first step toward developing a mechanistic tissue/tumor composition-based model for prediction of K_p values for tumors and antineoplastic drugs, with the aim of facilitating the use of PBPK models in oncology studies.

ACKNOWLEDGMENTS

This work represents an initiative undertaken in collaboration with Genentech, Inc. as a part of Dr. Poulin's research program. The authors kindly offer their gratitude to Hank La, Jonathan Cheong, Michelle Schweiger, and Emile Plise at Genentech, Inc. for their assistance, support, and contribution to the generation of the data; the authors also thank the Translational Oncology, In Vivo Studies and DMPK Groups at Genentech Inc. Finally, this work was performed in collaboration with the Dr. Seppänen-Laakso Tuulikki at the VTT Technical Research Centre of Finland, and Drs. Bhagwat Prasad and Jashvant D. Unadkat at the Department of Pharmaceutics at the University of Washington.

APPENDIX

This section contains the experimental settings used for the *in vivo* PK studies, *in vitro* transport studies and the analysis of tissue composition and transporter abundance.

In Vivo Studies

Cell Lines and Chemotherapy Agents

NCI-PC3 prostate cancer cells were obtained through a material transfer agreement between Genentech (South San Francisco, California) and the National Cancer Institute (Fredrick, Maryland). HCT 116 colon and NCI-H2122 non-small cell lung cancer cells were obtained from ATCC (Rockville, Maryland). Tumor cell lines were grown in RPMI 1640 media supplemented with 10% FBS, L-glutamine, and penicillin/streptomycin (Sigma–Aldrich, St. Louis, Missouri) at 37°C in 5% CO_2 and 95% air. NCI-PC3 cells were suspended in HBSS and HCT 116 and NCI-H2122 cells were suspended in HBSS–Matrigel (50:50) (BD Biosciences, Franklin Lakes, New Jersey) for injection in mice. Non-clinical grade DOC powder was synthesized by ChemShuttle for Genentech. GEM and adriamycin were obtained from SAGENT Pharmaceuticals (Schaumburg, Illinois), whereas MTX was obtained from Teva Pharmaceuticals (Netherlands). TOP was obtained from Bedford Laboratories (Bedford, Ohio).

PK Studies

All *in vivo* PK studies were approved by Genentech's Institutional Animal Care and Use Committee and adhere to the National Institutes of Health Guidelines for the Care and Use of Laboratory Animals. Human tumor xenografts for *in vivo* tissue distribution studies were established by subcutaneous injection of 5×10^6 NCI-PC3 cells, 5×10^6 HCT 116 cells, and 10×10^6 HCI-H2122 cells/female in NCR nude mice (Taconic, Germantown, New York). Animals were enrolled in treatment arms when tumors reached a volume of approximately 100–500 mm^3. Body weights and tumor volumes [caliper-based ellipsoid model: $L \times W$ 2/2, where the larger (L) and smaller (W) perpendicular dimensions are measured] were recorded 3 days prior to i.v. infusion. Animals were randomly assigned to treatment groups.

Intravenous Infusion

Mice bearing NCI-PC3, NCI-H2122, and HCT 116 xenografts were administered a single i.v. loading dose followed by a continuous i.v. infusion of chemotherapeutic agents at a rate of 80 μL/h. Chemotherapeutic agents were delivered by a jugular vein cannula that was surgically implanted 3 days and flushed with 0.9% sterile saline prior to infusion. Plasma, tumor, thigh muscle, subcutaneous adipose tissue, lung, liver, brain, and plasma ($n = 7$ mice per chemotherapeutic agent) were collected following a 7 h infusion with MTX (0.3731 mg/h) and GEM (1.3889 mg/h), an 8 h infusion with DOC (7.0 mg/h), a 17 h infusion with TOP (0.10 mg/h), and a 72 h infusion with adriamycin (0.0125 mg/h). Plasma samples of approximately 0.5 mL were collected from each mouse by terminal cardiac puncture following euthanasia by carbon dioxide inhalation. Blood samples were collected into tubes containing K_2EDTA as the anticoagulent. Samples were centrifuged within 1 h of collection and plasma was collected and stored at −80°C until analysis. Tissue samples were rinsed of extraneous blood with phosphate buffered saline, snap-frozen on dry ice, and stored at −80°C until analysis.

Tissue Sample Analysis

Sample Preparation

Tissue samples from mouse brain, fat, liver, lung, muscle, and tumor were homogenized using an Omni Bead Ruptor 24 homogenizer (Omni International, Kennesaw, Georgia). Four volumes of water (4 mL/g of tissue) was added to each tissue sample for homogenization except for the fat tissues for which four volumes of methanol/water (1:4, v/v) was added. Standard curves were prepared by spiking a known amount of DOC, DOX, GEM, MTX, or TOP into a blank tissue homogenate. Loperamide (20 ng/mL) was used as internal standard (IS) for the analysis of DOC, DOX, MTX, and TOP, and d_3-GEM (500 ng/mL) was used as IS for the analysis of GEM. Twenty five (25) microliters of samples or calibration standards was mixed with 5 μL of IS and 200 μL acetonitrile followed by vortexing and centrifugation at 1500*g* for 10–15 min. Fifty (50) microliters of supernatant of DOC, DOX, MTX, or TOP was diluted with 100 μL water and 10 μL diluted sample was injected to an ultra-performance liquid chromatography tandem mass spectrometry (UPLC–MS/MS) system for analysis. For GEM, 50 μL of supernatant was diluted with 150 μL acetonitrile and 1 μL of diluted sample was injected to an UPLC–MS/MS for analysis.

UPLC–MS/MS Methods

The UPLC–MS/MS system consisted of Nexera UHPLC system (Shimadzu, Columbia, Maryland) and an AB Sciex QTrap 5500 mass spectrometer (AB Sciex, Foster City, California). Separation of DOC, DOX, MTX, and TOP was achieved by reverse-phase liquid chromatograph. A Kinetex™ XB-C18, 2.6 μm, 50 × 2.1 mm^2 column (Phenomenex, Torrance, California) was used for DOC, DOX, and TOP and a Phenomenex Kinetex™ Phenyl-Hexyl, 2.6 μm, 50 × 2.1 mm^2 column was used for MTX. Mobile phases (MPs) were water containing 0.1% formic acid (A) and acetonitrile containing 0.1% formic acid (B). Gradient elution was ramped up from 20% MP B to 80% MP B for DOC and DOX, from 10% MP B to 85% MP B for MTX, and from 5% MP B to 85% MP B for TOP. Flow rate was 1.20 mL/min and run time was 0.8 min. Peak retention time was 0.49 min for DOC, 0.43 min for DOX, 0.42 min for MTX, and 0.43 min for TOP. For GEM, separation was achieved by hydrophilic interaction liquid chromatograph (HILIC) using a Halo Penta-HILIC, 2.7 μm, 50 × 2.1 mm^2 column (MAC-MOD, Chadds Ford, Pennsylvania). The MPs were water containing 5 mM ammonium acetate (A) and acetonitrile/water (99:1, v/v) containing 5 mM ammonium acetate (B). Gradient elution was ramped down from 100% MP B to 30% MP B at a flow rate of 1.20 mL/min. Run time was 1.2 min and peak retention time was 0.45 min.

Mass spectrometer parameters were optimized by infusing a neat solution of each compound and the IS separately. Ionization was achieved using a turbo-ionspray source operating in the positive ionization mode for all compounds and the IS. The quantitation was performed using the multiple reaction monitoring mode (MRM). The MRM transitions monitored were *m/z* 830.2–549.2 for DOC, 544.0–397.0 for DOX, 264.0–112.1 for GEM, 455.1–308.2 for MTX, 422.1–219.2 for TOP, 477.1–265.9 for loperamide (IS), and 267.0–115.1 for d_3-GEM (IS). Analyst software 1.4.2 was used to optimize the MS parameters, data acquisition, and data processing.

Standard curves were prepared in the range of 1.0–20,000 ng/mL. Samples were analyzed using two sets of standard curves in each analytical run. The lower limit of quantitation ranged from 1.0 to 9.1 ng/mL depending on the compound and tissue matrix. Concentrations of docetaxel, DOX, GEM, MTX, and TOP were calculated from the calibration line constructed from peak area ratios of the compound to the IS versus nominal compound concentrations with linear regression and $1/x^2$ or $1/x$ weighting. The assay accuracy was between 75% and 125%.

Tissue Composition Analysis

Homogenization of the Tissues

Before homogenization and analysis, the tissue samples were stored at −80°C. The samples from mouse liver, brain, lung, muscle, fat, and tumor tissues were homogenized (pulverized) as frozen (fast freezed in dry ice for 1 min) by using a Covaris CryoPrep System (Woburn, Massachusetts). The homogenates were transferred from TissueTubes™ into cryotubes for further storage at −80°C. Typically, 5 mg aliquots of pulverized samples were weighed for lipidomics analyses and 10 mg aliquots for other lipid determinations.

Lipid Extraction

For lipidomics profiling, pulverized tissue samples (5 mg) were spiked with an IS mixture (20 μL) consisting of lysophosphatidylcholine [LPC(17:0)], monoacylglycerol [MG(17:0/0:0/0:0)], phosphatidylglycerol [PG(17:0/17:0)], ceramide [Cer(d18:1/17:0)] phosphatidylcholine [PC(17:0/17:0)], phosphatidylethanolamine [PE(17:0/17:0)], diacyl-glycerol [DG(17:0/17:0)], triacylglycerol [TG(17:0/17:0/17:0)], cholesterylester [CE(19:0)], cardiolipin [CA(14:0)], C12(ß)-D-glucosyl ceramide, and C8 L-threo-lactosyl(ß)ceramide (d18:1/8:0) at concentration levels varying from 0.8 to 6.5 μg. Sodium chloride solution (15 mM, 50 μL) was added to the samples and lipids were extracted with a mixture of chloroform and methanol (2:1, 400 μL) by using a Retsch Mixer Mill homogenizer (Retsch GmbH, Haan, Germany) at −20°C for 2 min (20 Hz, two grinding balls Ø 3 mm). After 30–60 min extraction time at room temperature, the samples were centrifuged (Eppendorf 5804R) at 10,620*g* for 3 min. From the separated lower organic solvent layer, 200 μL was taken into a vial insert and mixed with 20 μL of a standard mixture containing three labeled lipid species: L-α-LPC palmitoyl-D3 (methyl-D3), 1,2-dipalmitoyl-D6–3-sn-glycero-phospha-tidylcholine (dimethyl-D6), and tripalmitin-1,1,1–^{13}C3 (concentration level 0.4–0.6 μg). Lipid extraction for fatty acid, Chol, and lipid class analyses was performed with chloroform–methanol (2:1, 800 μL) by using 10 mg of pulverized tissue samples mixed with 100 μL of 15 mM NaCl. After centrifugation and separation of the lower solvent layer, the extraction was repeated with 250 μL of chloroform–methanol (2:1). The extracts were combined, evaporated into dryness under nitrogen flow, and dissolved into 550 μL of chloroform.

Derivatization

For fatty acid analyses, 150 μL aliquots from the lipid extracts were spiked with triheptadecanoate [TG(17:0/17:0/17:0)] (18.7 μg/sample) and evaporated into dryness under nitrogen flow and dissolved into 500 μL of petroleum ether (bp

40°C–60°C). Lipids were transesterified with sodium methoxide by adding 250 μL of 0.5 N NaOMe in MeOH and a couple of boiling stones, and the mixture was boiled at 45°C for 5 min. The samples were acidified with 15% $NaHSO_4$ and the methyl esters as well as free fatty acids (FFAs) were extracted with petroleum ether. The separated petroleum ether layer was evaporated and dissolved into 50 μL of hexane. After analyzing fatty acid methyl esters (FAME) by GC, the same samples were trimethylsilylated to determine FFA and Chol contents. Samples were evaporated, dissolved into 30 μL dichloromethane (DCM) and silylated with 25 μL of MSTFA [N-methyl-N-(trimethylsilyl)trifluoroacetamide] at 80°C for 20 min.

Lipidomics (UPLC-QTof-MS)

Lipidomics runs were performed on a Waters Q-Tof Premier mass spectrometer combined with an Acquity Ultra Performance LC™ (UPLC). The column (at 50°C) was an Acquity UPLC™ ethylene bridged hybrid particle C18 2.1 × 100 mm^2 with 1.7 μm particles. The solvent system included ultrapure water (1% 1 M NH_4Ac, 0.1% HCOOH) and (B) acetonitrile/isopropanol (1:1, 1% 1 M NH_4Ac, 0.1% HCOOH, LC–MS grade). The gradient started from 65% A/35% B, reached 80% B in 2 min, 100% B in 7 min, and remained there for 7 min. The flow rate was 0.400 mL/min and the injected amount 2.0 μL (Acquity Sample Organizer, at 10°C). Reserpine was used as the lock spray reference compound. The lipid profiling was carried out in electrospray ionization (ESI) positive mode and the data (centroid) was collected at a mass range of *m/z* 300–1200 with scan duration of 0.2 s. The samples were further run in ESI negative mode at a mass range of *m/z* 300–2000 to detect CAs. The peaks were measured by using peak heights. The lipidomics data were processed by using MZmine 2 software (mzmine.sourceforge.net) including alignment of peaks, peak integration, healthyization, and peak identification. Lipids were identified using an internal spectral library. Quantification of lipid subspecies was based on peak heights of ISs. All monoacyl lipids except Chol esters, such as MGs and monoacylglycerophospholipids, were healthyized with PC(17:0/0:0), all diacyl lipids except ethanolamine phospholipids were healthyized with PC(17:0/17:0), all ceramides with Cer(d18:1/17:0), all diacyl ethanolamine phospholipids with PE(17:0/17:0), and TGs and CEs were healthyized with TG(17:0/17:0/17:0) and CE(19:0), respectively. Other (unidentified) molecular species were healthyized with PC(17:0/0:0) for retention time <300 s, PC(17:0/17:0) for retention time between 300 s and 410 s, and TG(17:0/17:0/17:0) for higher retention times.

Fatty Acid and Chol Analyses (GC–MS)

FAMEs were analyzed on an Agilent 7890A GC combined with an Agilent 5975C mass selective detector. The column was an Agilent FFAP silica capillary column (25 m × 0.2 mm × 0.3 μm). Helium was used as carrier gas with a split ratio of 15:1. The oven temperature programme was from 70°C (2 min) to 235°C at a rate of 10°C/min, total run time was 30 min. The temperatures of the injector and MS source were 220°C and 230°C, respectively. The samples (2 μL) were injected by a Gerstel MPS injection system and the data were collected in electron impact mode (70 eV) at a mass range of *m/z* 40–600. FAMEs with chain length from C14 to C22 were quantified in all samples. Trimethylsilylated samples were analyzed on a Restek Rtx®-5MS column (15 m × 0.25 mm × 0.25 μm). The split ratio was 20:1 and the oven temperature programme from 70°C (1 min) to 270°C at a rate of 10°C/min, the total run time was 30 min. In addition to FFAs and Chol, TG-based ether bonded lipids were silylated and detected (*m/z* 205, molecular ions). FFAs C16:0, C18:0, C18:1, and C18:2 were quantified in all samples and ether bonded lipids C16:0, C18:0, and C18:1 in lung, fat, and tumor tissue samples.

Analysis of Lipid Classes (HPLC–ELSD)

The lipid class analyses were performed on a Waters Alliance HPLC combined with a Cunow DDL21 evaporative light scattering detector (ELSD). Separation of the lipid classes was carried out on a Waters Spherisorb® silica column (5 μm, 150 × 4.6 mm I.D.). The gradient system consisted of (A) MTBE (methyl *tert*-butyl ether)–tetrahydrofurane (99:1), (B) 2-propanol-DCM (DCM; 4:1), and (C) 2-propanol-water (1:1) containing triethylamine and formic acid (50 μmol). The temperature of the detector was 40°C and air flow 27 psi. The multigradient system started from 100% A, the proportion of A decreased to 32%, that of B increased to 52%, and simultaneously that of the water containing C increased to 16%. Keeping the cycle running continuously enabled stabile retention times. The injection volume was 30 μL. Lipid classes were quantified by using calibration curves obtained from dilution series of C17:0 pure compounds: PC, LPC, PE, LPE, CA, SPH, PS, PI, PG, PA, Cer, sulfatides, and Cerebr. In order to improve the response and quantification of acidic phospholipids, especially PS, the samples were run also by slightly modifying the solvent system used by Homan and Anderson.[27] Solvent A consisted of iso-octane and tetrahydrofurane (99:1), solvent B of acetone and DCM (2:1), and C of 2-propanol and water (85:15). Solvent C contained acetic acid (750 μL/L) and triethylamine (250 μL/L), the pH of the solvent was 4.5. Tumor tissue extracts were concentrated 5×, other tissue extracts 2×, and 20 μL aliquots were injected.

Transporter Abundance Analyses

The membrane protein extraction and total protein quantification procedure for the human tumor xenografts are the same as that one described in a recent publication.[28]

In Vitro Transport Studies

MDR1-MDCKI and MDCKII-MBCRP cells were licensed from the NCI (National Cancer Institute, Bethesda, Maryland). For transport studies, cells were seeded on 24-well Millicell plates (Millipore, Billerica, Massachusetts) 4 days prior to use (polyethylene terephtalate membrane, 1 μM pore size) at a seeding density of 1.2×10^5 cells/mL. Compounds were tested at 5 μM in the apical to basolateral (A–B) and basolateral to apical (B–A) directions. The compounds were dissolved in transport buffer consisting of Hank's balanced salt solution with 10 mM HEPES (Invitrogen Corporation, Grand Island, New York). Lucifer Yellow (Sigma–Aldrich) was used as the paracellular marker. Compound concentrations in the donor and receiving compartments were determined by LC–MS/MS analysis. The apparent permeability (P_{app}) values in the A–B and B–A directions were calculated after a 3-h incubation as:

$$P_{app} = (dQ/dt)(1/AC_0) \quad (1)$$

where A, surface area of the insert; C_0, initial substrate concentration at T_0; dQ/dt, rate of compound appearance in the receiver compartment. The efflux ratio was calculated as P_{app}, B–A/P_{app}, A–B.

REFERENCES

1. Tarique I, Venkateshan SP, Tandon M, Nilanjan S, Pillai KK. 2011. Comparative evaluation of US Food and Drug Administration and pharmacologically guided approaches to determine the maximum recommended starting dose for first-in-human clinical trials in adult healthy men. Clin Pharmacol 51:1655–1664.

2. Mariappan TT, Mandlekar S, Marathe P. 2013. Insight into tissue unbound concentration: Utility in drug discovery and development. Curr Drug Metab 14:324–340.

3. Poulin P, Hop ECA, Salphalti L, Liederer B. 2013. Correlation of tissue:plasma partition coefficient between healthy tissues and subcutaneous xenografts of human tumor cell lines in mouse as a prediction tool of drug penetration in tumors. J Pharm Sci 102:1355–1369.

4. Poulin P, Dambach DM, Hartley DH, Ford K, Theil FP, Harstad E, Halladay J, Choo E, Boggs K, Liederer BM, Dean B, Diaz D. 2013. An algorithm for evaluating potential tissue drug distribution in toxicology studies from readily available pharmacokinetic parameters. J Pharm Sci 102:3816–3829.

5. Haritova AM, Fink-Gremmels J. 2010. A simulation model for the prediction of tissue:plasma partition coefficients for drug residues in natural casings. The Vet J 185:278–284.

6. Richter W, Starke V, Whitby B. 2006. The distribution pattern of radioactivity across different tissues in quantitative whole-body autoradiography (QWBA) studies. Eur J Pharm Sci 28 :155–165.

7. Poulin P, Theil FP. 2000. *A priori* prediction of tissue:plasma partition coefficients of drugs to facilitate the use of physiologically based pharmacokinetic models in drug discovery. J Pharm Sci 89:16–35.

8. Poulin, P, Theil FP. 2009. Development of a novel method for predicting human volume of distribution at steady-state of basic drugs and comparative assessment with existing methods. J Pharm Sci 98:4941–4961.

9. Poulin P, Ekin, S, Theil FP. 2011. A hybrid approach to advancing quantitative prediction of tissue distribution of basic drugs in human. Toxicol Appl Pharmacol 250:194–212.

10. Björkman S. 2002. Prediction of the volume of distribution of a drug: Which tissue:plasma partition coefficients are needed? J Pharm Pharmacol 54:1237–1245.

11. Jansson R, Bredberg U, Ashton M. 2008. Prediction of drug tissue to plasma concentration ratios using a measured volume of distribution in combination with lipophilicity. J Pharm Sci 97:2324–2339.

12. Edginton AN, Yun YE. 2013. Correlation-based prediction of tissue-to-plasma partition coefficients using readily available input parameters. Xenobiotica 43:839–852.

13. Yoshida M, Kobunai T, Aoyagi K, Saito H, Utsugi T, Wierzba K, Yamada Y. 2000. Specific distribution of TOP-53 to the lung and lung-localized tumor is determined by its interaction with phospholipids. Clin Cancer Res 6:4396–4401.

14. Yata N, Toyoda T, Murakami T, Nishura A, Higashi Y. 1999. Phosphatidylserine for the tissue distribution of weakly basic drugs in rats. Pharm Res 7:1019–1025.

15. Peyret T, Poulin P, Krishnan K. 2011. A unified algorithm for predicting partition coefficients for PBPK modeling of drugs and environmental chemicals. Toxicol Appl Pharmacol 249:197–207.

16. Rodgers T, Rowland M. 2006. Physiologically-based pharmacokinetics modeling 2: Predicting the t issue distribution of acids, very weak bases, neutrals and zwitterions. J Pharm Sci 95:1238–1252.

17. Mairinger S, Erker T, Müller M, Langer O. 2011. PET and SPECT radiotracers to assess function and expression of ABC transporters in vivo. Curr Drug Metab 12:774–792.

18. Hudachek S, Gustafson DL. 2013. Incorporation of ABCB1-mediated transport into a physiologically-based pharmacokinetic model of docetaxel in mice. J Pharmacokinet Pharmacodyn 40:437–449.

19. Martignoni M, de Kanter R, Moscone A, Grossi P, Monshouwer M. 2005. Lack of strain-related differences in drug metabolism and efflux transporter characteristics between CD-1 and athymic nude mice. Cancer Chemother Pharmacol 55:129–135.

20. Drug bank. Assessed June 22, 2014, at: http://www.drugbank.ca/drugs.

21. Product Monograph. Topetacan hydrochloride for injection; Hycamtin. Version 5. November 20th 2013. Uxbridge, Middlesex, UK: GlaxoSmithKline, UB11 1BT.

22. Bradshaw-Pierce EL, Eckhardt SG, Gustafson D. 2007. A physiologically-based pharmacokinetic model of Docetaxel disposition: From mouse to man. Clin Res Cancer 13:2768–2776.

23. Mosure KW, Henderson AJ, Klunk LW, KNipe JO. 1997. Disposition of conjugate-bound and free doxorubicin in tumor-bearing mice following administration of a BR96-doxorubicin immunoconjugate (BMS 182248). Cancer Chemother Pharmacol 40:251–258.

24. Sani SN, Henry K, Boehlke JK, Stricker-Krongrad A, Maher TJ. 2010. The effects of drug transporter inhibitors on the pharmacokinetics and tissue distribution of methotrexate in healthy and tumor-bearing mice: A microdialysis study. Cancer Chemother Pharmacol 66:159–169.

25. Shah DK, Balthasar JP. 2011. Physiologically-based pharmacokinetic model for topotecan in mice. J Pharmacokinet Pharmacodyn 38:121–142.

26. Beumer JH, Eiseman JL, Parise RA. 2008. Modulation of Gemcitabine (2,2-difluoro-2-deoxycytidine) pharmacokinetics, metabolism, and bioavailability in mice by 3,4,5,6-tetrahydrouridine. Clin Cancer Res 14:3529–3535.

27. Homan R, Anderson MK. 1998. Rapid separation and quantification of combined neutral and polar lipid classes by high-performance liquid chromatography and evaporative light-scattering mass detection. J Chromatogr B 708:21–26.

28. Prasad B, Evers R, Gupta A, Hop ECA, Salphati L, Shukla S, Ambudkar S, Unadkat JD. 2014. Interindividual variability in hepatic organic anion-transporting polypeptides and P-glycoprotein (ABCB1) protein expression: Quantification by liquid chromatography tandem mass spectroscopy and influence of genotype, age, and sex. Drug Metab Dispos 42:78–88.

29. Huxham LA, Kyle AH, Baker JHE, et al. 2004. Microregional effects of gemcitabine in HCT-116 xenografts. Cancer Res 64:6537–6541.

30. Ojugol ASE, McSheehy PMJ, Stubbs M, Alder G, Bashford CL, Maxwell RJ, Leach MO, Judson IR, Griffiths GR. 1998. Influence of pH on the uptake of 5-fluorouracil into isolated tumour cells. Br J Cancer 77:873–879.

31. Lyng H, Tufto I, Skretting A, Rofstad EK. 1997. Proton relaxation times and interstitial fluid pressure in human melanoma xenografts. Br J Cancer 75:180–183.

32. Berk DA, Yuan F, Leunig M, Rakesh KJ. 1997. Direct in vivo measurement of targeted binding in a human tumor xenograft. Proc Natl Acad Sci USA 94:1785–1790.

33. Boswell AC, Ferl GZ, Mundo EE, Bumbaca D, Schweiger MG, Theil FP, Fielder PJ, Khawli LA. 2011. Effects of Anti-VEGF on predicted antibody biodistribution: Roles of vascular volume, interstitial volume, and blood flow. PLoS One 6:e17874.

34. Raghunand N, Altbach MI, Van Sluis R, Baggett B. 1999. Plasmalemmal pH-gradients in drug-sensitive and drug-resistant MCF-7 human breast carcinoma xenografts measured by 31P magnetic resonance spectroscopy. Biochem Pharmacol 57:309–312.

35. Calderwood SK, Dickson JA. 1980. Effect of hyperglycemia on blood flow, pH, and response to hyperthermia of the yoshida sarcoma in the rat. Cancer Res 40:4728–4733.

36. Gerweck LE, Seetharaman K. 1996. Cellular pH gradient in tumors versus healthy tissues: Potential exploitation for the treatment of cancer. Cancer Res 56:1194–1198.

37. Tsukamoto Y, Kato Y, Ura M, Horii I, Ishikawa T, Ishitsuka H, Sugiyama Y. 2001. Investigation of 5-FU disposition after oral administration of capecitabine, a triple-prodrug of 5-FU, using a physiologically based pharmacokinetic model in a human cancer xenograft model: Comparison of the simulated 5-FU exposures in the tumour tissue between human and xenograft model. Biopharm Drug Dispos 22:1–14.
38. Thurber GM, Weissleder R. 2011. A systems approach for tumor pharmacokinetics. PLoS One 6:e24696.
39. Huang Y, Sadée W. 2006. Membrane transporters and channels in chemoresistance and sensitivity of tumor cells. Cancer Lett 239:168–182.
40. Scotto KW. 2003. Transcriptional regulation of ABC drug transporters. Oncogene 22:7496–7511.
41. Cisternino S, Bourasset F, Archimbaud Y, Semiond D, Sanderink G, Scherrmann JM. 2003. Nonlinear accumulation in the brain of the new taxoid TXD258 following saturation of P-glycoprotein at the blood–brain barrier in mice and rats. Br J Pharmacol 138:1367–1375.
42. Kalvass JC, Polli JW, Bourdet DL, Feng B, Huang SM, Liu X, Smith QR, Zhang LK, Zamek-Gliszczynski MJ. 2013. Why clinical modulation of efflux transport at the human blood–brain barrier is unlikely: The ITC evidence-based position. Nature 94:80–94.
43. Uchida Y, Ohtsuki S, Kamiie J, Terasaki T. 2011. Blood-brain barrier (BBB) pharmacoproteomics: Reconstruction of in vivo brain distribution of 11 P-Glycoprotein substrates based on the BBB transporter protein concentration, in vitro intrinsic transport activity, and unbound fraction in plasma and brain in mice. J Pharmacol Exp Ther 339:579–588.
44. Agarwal S, Uchida Y, Mittapalli RK, Sane R, Terasaki T, Elmquist WF. 2011. Quantitative proteomics of transporter expression in brain capillary endothelial cells isolated from P-gp, Bcrp, and P-gp/Bcrp knockout mice. Drug Metab Dispos 40:1164–1169.
45. Bleasby K1, Castle JC, Roberts CJ, Cheng C, Bailey WJ, Sina JF, Kulkarni AV, Hafey MJ, Evers R, Johnson JM, Ulrich RG, Slatter JG. 2006. Expression profiles of 50 xenobiotic transporter genes in humans and pre-clinical species: A resource for investigations into drug disposition. Xenobiotica 36:963–988.
46. Venishetty VK, Komuravelli R, Kuncha M, Sistla R, Diwan PV. 2013. Increased brain uptake of docetaxel and ketoconazole loaded folate-grafted solid lipid nanoparticles. Nanomedicine 9:111–121.
47. Davis JR, Fernandes C, Zalcberg JR. 1999. Gemcitabine and the blood brain barrier. Aust NZ J Med 6:831–832.
48. Rousselle C, Clair P, Lefauconnier JM, Kaczorek M, Scherrmann JM, Temsamani J. 2000. New advances in the transport of doxorubicin through the blood-brain barrier by a peptide vector-mediated strategy. Mol Pharmacol 4:679–686.
49. Blakeley JO, Olson J, Grossman SA, He X, Weingart J, Supko JG. 2009. Effect of blood brain barrier permeability in recurrent high grade gliomas on the intratumoral pharmacokinetics of methotrexate: A microdialysis study. J Neurooncol 91:51–58.
50. Zhuang Y, Fraga CH, Elaine KH, Hagedorn N, Panetta JC. Et al. 2006. Topotecan central nervous system penetration is altered by a tyrosine kinase inhibitor. Cancer Res 66:23–33.
51. Taskar KS, Rudraraju V, Mittapalli RK, Samala R, Thorsheim HR, Lockman J, Gril B, Emily H, Palmieri D, Polli, et al. 2012. Lapatinib distribution in HER2 overexpressing experimental brain metastases of breast cancer. Pharm Res 29:770–781.
52. Lv H, Zhang X, Sharma J, Reddy MVR, Reddy EP, Gallo JM. 2012. Integrated pharmacokinetic-driven approach to screen candidate anticancer drugs for brain tumor chemotherapy. AAPS J 15:250–257.
53. Zlatopolskiy BD, Morgenroth A, Kunkel FH, Urusova EA, Dinger C, Kull T, Lepping C, Reske SN. 2009. Synthesis and biologic study of IV-14, a new ribonucleoside radiotracer for tumor visualization. J Nucl Med 50:1895–1903.
54. Pennycooke M, Chaudary N, Shuralyova I, Zhang Y, Coe IR. 2001. Differential expression of human nucleoside transporters in normal and tumor tissue. Biochem Biophys Res Commun 26:951–959.
55. Cottin S, Ghani K, Campos-Lima OP, Caruso M. 2010. Gemcitabine intercellular diffusion mediated by gap junctions: New implications for cancer therapy. Mol Cancer 9:141.
56. Tannock Ian F, Lee Carol M, Tunggal Jonathon K et al. 2002. Limited penetration of anticancer drugs through tumor tissue: A potential cause of resistance of solid tumors to chemotherapy. Clin Cancer Res 8:878–884.
57. Hill R, Rabb M, Madureira PA, Clements D, Gujar SA, Waisman DM, Giacomantonio CA, Lee PWK. 2013. Gemcitabine-mediated tumour regression and p53-dependent gene expression: Implications for colon and pancreatic cancer therapy. Cell Death Dis 4:e791.
58. Goricar K, Kovac V, Dolzan V. 2014. Polymorphisms in folate pathway and pemetrexed treatment outcome in patients with malignant pleural mesothelioma. Radiol Oncol 48:163–172.
59. Hanumegowda UM, Wenke G, Regueiro-Ren A, Yordanova R, Corradi JP, Adams SP. 2010. Phospholipidosis as a function of basicity, lipophilicity, and volume of distribution. Chem Res Toxicol 23:749–755.
60. Lullmann H, Rossen E, Seiler KU. 1972. The pharmacokinetics of phentermine and chlorphentermine in chronically treated rats. J Pharm Pharmacol 25:239–243.
61. Wong H, Choo EF, Alicke B, et al. 2012. Antitumor activity of targeted and cytotoxic agents in murine subcutaneous tumor models correlates with clinical response. Clin Cancer Res 18:3846–3855.
62. Rodgers T, Jones HM, Rowland M. 2012. Tissue lipids and drug distribution: Dog versus rat. J Pharm Sci 101:4615–4625.